journal

Reprinted from the Journal of the American Ceramic Society, Vol. 76, No. 9, September 1993
Copyright © 1993 by The American Ceramic Society
J. Am. Ceram. Soc., 76 [9] 2241–47 (1993)

Model for Toughness Curves in Two-Phase Ceramics: II, Microstructural Variables

Nitin P. Padture,*,† Julie L. Runyan,‡ Stephen J. Bennison,*,§ Linda M. Braun,* and Brian R. Lawn*

Ceramics Division, Materials Science and Engineering Laboratory, National Institute of Standards and Technology, Gaithersburg, Maryland 20899

The fracture mechanics analysis of Part I is here extended to consider the effects of volume fraction and scale of second-phase particles on the toughness-curve properties of ceramic-matrix composites. Increasing these variables enhances the flaw tolerance of the material, but only up to certain limits, beyond which bulk microcracking occurs. These limits define domains of damage accumulation and potential strength degradation by microcrack coalescence. In the familiar approximation of elliptical crack-wall profiles, we show that the principal effects of increasing volume fraction (or expansion mismatch) and particle size is to enhance the *slope* and *scale* of the *T*-curve, respectively. We also derive expressions for the microcracking limits and use these expressions to construct a simple design diagram for characterizing the effects of microstructural variation on mechanical behavior. Indentation–strength data on Al_2O_3/Al_2TiO_5 composites over a range of volume fractions and particles sizes are used to demonstrate the severe loss in mechanical integrity that can be suffered on entering the microcracking domains.

I. Introduction

In PART I,[1] we developed a simplified fracture mechanics toughness-curve (*T*-curve) model for two-phase ceramics. Experimental indentation–strength data on an alumina-matrix/aluminum titanate (Al_2O_3/Al_2TiO_5) particle-reinforced composite were used to confirm the essential features of the model and to calibrate controlling microstructural parameters for the *T*-curve. We are now placed to predict the effects of specified microstructural change on the toughness and strength properties of that composite system.

Accordingly, in Part II we investigate the predictive capacity of the model by analyzing the effects of volume fraction V_f and particle size l of the second phase, in addition to matrix/particle expansion mismatch stress σ_R, on the toughness. We shall show that increasing V_f (or σ_R) and l, respectively, enhances the slope and scaling characteristics of the *T*-curve, with profound consequences concerning crack stability. Beyond critical compositions the material is able to sustain multiple flaw extension prior to failure. This is the domain of microcrack damage accumulation and nonlinear stress–strain response. At even higher V_f and l, the strength is severely degraded, indicative of microcrack coalescence. Indentation–strength tests on Al_2O_3/Al_2TiO_5 composites with different volume fractions and particle sizes are used to validate these predictions.

The model will be discussed in special relation to microstructural strategies for optimum toughness characteristics, in terms of a simple design diagram.

II. Effect of Microstructural Variables on Toughness and Strength

Using the "calibrated" *T*-curve, $T(c)$, function for the reference composite material of Part I, we set out to predict the influence of two major microstructural variables, volume fraction V_f and particle diameter l, on the indentation–strength characteristics. Internal residual stress σ_R is also a parameter of potential interest, but that quantity is invariant for a given matrix–particle composite system. We again address the specific configuration of a half-penny crack in a semi-infinite medium.

(1) *Microstructure Parametric Relations*

In this subsection we seek relations between V_f and l and the controlling microstructural parameters in the $T(c)$ formalism of Section II, Part I: i.e., shielding stresses p and q, and bridging zone dimensions λ and Λ.

The microstructural dependence of the shielding stresses is given by Eqs. (2) and (3), Part I:

$$q = \frac{1}{2}V_f(1 - V_f)\sigma_R \qquad (0 \le 2u \le \varepsilon_\delta l) \qquad (1a)$$

$$p = \frac{1}{2}\eta\mu\varepsilon_\xi V_f(1 - V_f)\sigma_R \qquad (\varepsilon_\delta l \le 2u \le \varepsilon_\xi l) \qquad (1b)$$

with η a microstructural geometry parameter, μ a friction coefficient, and ε_δ and ε_ξ size-independent strains at which the bridging particle relaxes its elastic crack-opening stresses and disengages from the matrix, respectively. Eqs. (1*a*) and (1*b*) are basic microstructural *stress* relations for the *T*-curve. Observe that p and q depend on V_f (and σ_R), but not on l.

Analogous microstructural dependencies of λ and Λ can be obtained from Eq. (3), Part I, but less directly, requiring relations between λ and δ, Λ and ξ. It is now necessary to introduce appropriate crack-opening displacement relations. To maintain an equilibrium state, these relations must be solved simultaneously and self-consistently with the *K*-field condition $K_A(c) = T(c)$ in Eq. (6) of Part I, using Eq. (8) in Part I to evaluate $T(c)$ in the appropriate crack-size domains. Generally, such crack-opening displacement relations are couched in a nonlinear integral equation formalism.[2–4] In the present study, in the interest of maintaining simplicity, we use first-order solutions for strictly *uniform* stresses over the *entire* crack plane, i.e., elliptical profiles,[2] giving

$$\delta = (2\psi T_0/E')(2\lambda)^{1/2} \qquad (2a)$$

$$\xi = (2\psi T_0/E')(2\Lambda)^{1/2} \qquad (\lambda << \Lambda) \qquad (2b)$$

D. K. Shetty—contributing editor

Manuscript No. 195173. Received October 27, 1992; approved May 28, 1993.
Supported by the Air Force Office of Scientific Research and E. I. duPont Nemours and Company, Inc.
*Member, American Ceramic Society.
†Guest Scientist, from Department of Materials Science and Engineering, Lehigh University, Bethlehem, PA 18015.
‡Now at School of Materials Engineering, Georgia Institute of Technology, Atlanta, GA 30332.
§Now at Experimental Station, E. I. duPont Nemours and Company, Wilmington, DE 19880-0356.

with $E' = E(1 - \nu^2)$, E Young's modulus and ν Poisson's ratio, and T_0 the matrix (grain boundary) toughness, again regarding λ and Λ as constants for a given microstructure.

Of course, the actual internal stress distribution over the crack plane in Fig. 3, Part I, is highly *non*uniform, with discontinuities in stress and stress gradient at $r = \lambda$. In reality, relative to the profile solutions of Eq. (2), the walls will bulge open in the opening-stress domain $c - \lambda \leq r \leq c$ immediately behind the tip and, conversely, pinch down in the more remote closure-stress domain $c - \Lambda - \lambda \leq r \leq c - \lambda$.[5] Under such conditions, neither λ nor Λ will be strictly independent of p and q (hence V_f), or even of c (until one satisfies the requirements of the "small-zone" approximation $\lambda << \Lambda << c$[6]). Here, even though the displacement field equations are actually integrable for the stresses shown in Fig. 3 of Part I,[5,7,8] we choose to avoid such complexities in order to bring out the essential microstructural dependence of the T-curve more clearly.

Inversion of Eq. (2), in conjunction with Eq. (3) of Part I, yields relations

$$\lambda = \frac{1}{2}(\varepsilon_\delta E'/2\psi T_0)^2 l^2 \qquad (3a)$$

$$\Lambda = \frac{1}{2}(\varepsilon_\xi E'/2\psi T_0)^2 l^2 \qquad (\lambda << \Lambda) \qquad (3b)$$

which (neglecting any influence of the second phase on E') are independent of V_f (and also σ_R) and c, but scale with l. Equations (3a) and (3b) are basic microstructural *scaling* relations for the T-curve. Note that $\Lambda/\lambda = (\varepsilon_\xi/\varepsilon_\delta)^2 =$ constant, independent of V_f (and σ_R) and l; i.e., Λ and λ scale similarly with any change in the particle size.

(2) *Damage Accumulation by General Microcracking*

In our concluding remarks to Part I we alluded to a potential transition in flaw stability, depending on whether the extrapolated intercept of the "linear" T–$c^{1/2}$ function (Eq. (9), Part I) on the T-axis is positive or negative. The critical, zero-intercept transition condition is illustrated in the schematic of Fig. 1, where $T(c)$ is plotted as the solid curve. Let us consider intrinsic flaws that are free of spurious residual stresses (i.e., $\chi = 0$ in Eq. (11), Part I), and that have evolved fully through the bridging field from inception. Then the origin of the $K_A(c)$ function, $K_A' = K_A = \psi\sigma_A c^{1/2}$ in Eq. (12), Part I, plotted as the shaded line in Fig. 1, coincides with that of the linear T–$c^{1/2}$ function. Using this critical transition configuration as a reference state, and supposing the material to contain at least a proportion of flaws of initial size $c = c_f$ within the two vertical dashed lines in Fig. 1, we may usefully delineate the following regions of stability:

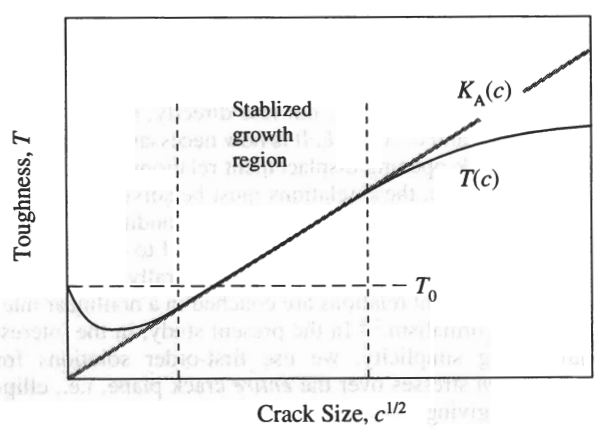

Fig. 1. Schematic diagram showing T-curve construction at limit of bulk microcrack activation. Solid curve is $T(c)$ at critical condition given by Eq. (6), shaded line is $K_A = \psi\sigma_A c^{1/2}$. Any flaw of initial size within the two vertical dashed lines will extend stably along the T-curve to failure at the extreme right dashed line.

(A) Positive Intercept, No Microcracking: For a material with positive intercept, such as our reference material in Fig. 6 of Part I, the equilibrium configuration $K_A = \psi\sigma_A c_f^{1/2} = T$ corresponds to a slope $dK_A/d(c^{1/2}) > dT/d(c^{1/2})$. Failure then occurs abruptly and unstably from a single critical flaw at $c = c_f$. Nevertheless, the material shows flaw tolerance, because the toughness T at failure effectively increases with c_f. For systems *just* at the transition in Fig. 1, the strength becomes altogether independent of c_f; i.e., the equilibrium is neutral. The applied stress–strain response is linear in this region.

(B) Negative Intercept, Activated Microcracking: For a material with negative intercept the condition $K_A = T$ at $c = c_f$ corresponds to a slope $dK_A/d(c^{1/2}) < dT/d(c^{1/2})$. The flaw then undergoes a precursor stage of stable extension with increasing σ_A, until a tangency condition $dK_A/d(c^{1/2}) = dT/d(c^{1/2})$ is met. The strength σ_F for breaks from natural flaws is now altogether independent of c_f. In this region, even though failure still occurs from a single critical flaw, other flaws may nevertheless undergo significant prefailure extension. This can result in accumulation of microcrack damage through the material prior to failure, the more so as the negative intercept increases. The applied stress–strain response of the material now becomes nonlinear.

(C) Negative Intercept, Spontaneous Microcracking: With still further depression of the negative intercept, such that the minimum in the T-curve falls below the c-axis, the system enters a severe-damage domain in which flaw pop-in can occur in the absence of applied stress, increasing the density of stable flaws and further enhancing the stress–strain nonlinearity.

The configuration of Fig. 1 delineating the transition between states (A) and (B) above corresponds to a critical volume fraction V_f^* (or residual stress σ_R^*) at fixed l, or to a critical particle size l^* at fixed V_f. This critical condition may be formalized by requiring $T = 0$ at $c = 0$ in the $T(c)$ function of Eq. (9) in Part I, yielding

$$[(p + q)(2\lambda)^{1/2}]^* = T_0/\psi \qquad (4)$$

Invoking Eqs. (1) and (3) above allows us to express Eq. (4) in terms of microstructural variables,

$$[V_f(1 - V_f)l\sigma_R]^* = 4T_0^2/(1 + \eta\mu\varepsilon_\xi)\varepsilon_\delta E' \qquad (5)$$

Hence, damage accumulation may be promoted by increasing the volume fraction (or residual internal stress) or scaling up the particle size.

An analogous condition for spontaneous microcracking may be obtained by requiring the minimum in the $T(c)$ function to intersect the c-axis. Approximating this minimum as the intersection point of the T–$c^{1/2}$ functions in Eqs. (8a) and (9) in Part I, i.e., $T = 0$ at $c \approx 2\lambda$, we have

$$[q(2\lambda)^{1/2}]^{**} = T_0/\psi \qquad (6)$$

Again invoking Eqs. (1) and (3), we obtain

$$[V_f(1 - V_f)l\sigma_R]^{**} = 4T_0^2/\varepsilon_\delta E' \qquad (7)$$

which is greater than $[V_f(1 - V_f)l\sigma_R]^*$ in Eq. (5) by a factor $1 + \eta\mu\varepsilon_\xi$ (neglecting any reduction in E' from the microcracking). The latter factor therefore defines a "window" of activated damage.

In the nonlinear region lower-bounded by Eq. (5), the prospect exists for coalescence of the stable microcracks, with attendant strength degradation. Coalescence is a "many-body" problem, depending on the characteristic spacing between neighboring, interactive microcrack sources in an actively evolving population. There is therefore a stochastic element in the mechanics of damage accumulation. Here we simply note that if the source–source spacing is less than the fully extended flaw size at the critical tangency condition, the strength drop will tend to be immediate. If the sources are more distantly spaced, the drop-off will be more gradual. Any remaining strength after coalescence will depend on the *variability* in the spatial distribution of the sources.

III. Microcracking Limits of Al_2O_3/Al_2TiO_5 Composites: Analysis Using Indentation–Strength Data

(1) Experimental Procedure

We now investigate the predictions of the T-curve analysis using indentation–strength data for Al_2O_3/Al_2TiO_5 composites of different volume fraction and particle size of the Al_2TiO_5 phase.

Materials were prepared as described in Section III(1) of Part I. Batches of material were fabricated with volume fractions $V_f = 0.10$, 0.20, 0.30, and 0.40, by altering the starting powder composition. Specimens from each batch were then heat-treated over a range of aging times[9] to grow the Al_2TiO_5 particles from their initial size, $l < 2$ μm, over a range of sizes up to a maximum $l = 12$ μm. The matrix grains were observed to scale similarly, but remained within a range of negligible influence on the T-curve.[10]

Strength tests were carried out as in Part I. Disks for strength testing were polished, then indented with a Vickers diamond at a prescribed load $P = 5$ N. This load is close to the intersection point of data sets for the reference composite and base alumina in Fig. 5 of Part I, i.e., in a region where the strength is relatively material-insensitive. The disks were then broken in biaxial flexure to obtain inert strength data. Post-mortem examinations were again made of all broken specimens to confirm failure initiation from the indentation sites. Means and standard deviations in strengths were evaluated from 4–6 tests at each value of V_f and l, where possible; beyond the strength falloff limits (Sect. III(2)), the success rate for breaks at indentations diminished rapidly, and the data were most often restricted to individual breaks.

Some of the specimen surfaces were examined for evidence of microcracking, both before and after strength testing.

(2) Influence of Volume Fraction and Particle Size on Microcracking Limits

Figure 2 plots the indentation–strength data as a function of particle size, $\sigma_M(l)$, at each of the volume fractions $V_f = 0.10$, 0.20, 0.30, 0.40. We see that, generally, σ_M falls off with l, initially slowly and thereafter, beyond a cutoff, precipitously. Increasing V_f shifts the "cliff" progressively to the left of the plots.

Surface examinations of the specimens showed a correlation between position on the strength plots in Fig. 2 and the incidence of microcracking. At the top of the cliff, the specimens gave no indication of multiple flaw extension. In this region the applied load–displacement curve remained essentially linear. Over the edge of the cliff, sporadic microcracking could be detected in the broken specimens using scanning electron microscopy. At the bottom of the cliff, microcracking was more prevalent, and the applied load–displacement curve showed nonlinearity[9]—in this domain the material may be considered to be "overaged". An example of spontaneous microcracking in a heavily overaged material is shown in Fig. 3. Materials subjected to even more overaging were so heavily microcracked that, on prolonged exposure (i.e., several days) to moist atmospheres, they began to crumble, with virtually total loss of strength.

The solid curves at left in each plot are calculated from the theoretical indentation–strength analysis (Sect. II(3), Part I). For these calculations, we use the previously defined indentation coefficients $\psi = 0.77$ and $\chi = 0.076$, and alumina matrix toughness $T_0 = 2.75$ MPa·m$^{1/2}$ (Ref. 11) (Sect. III(2), Part I). We also use the microstructural parameters $p = 325$ MPa, $(p + q)(2\lambda)^{1/2} = 3.51$ MPa·m$^{1/2}$ and $\Lambda = 180$ μm (Eq. (17), Part I) defined for our reference composite ($V_f = 0.20$, $l = 4.0$ μm); Eq. (1) is then invoked to scale the bridging stresses p and q for each new V_f, and Eq. (3) to scale bridging zone dimensions λ and Λ for each new l.

Beyond a critical particle size l^* at each V_f, evaluated by setting $V_f(1 - V_f)l^* = 0.672$ μm in accordance with Eq. (5), we approximate the strength degradation as an infinitely abrupt falloff, indicated by the *left*-hand vertical dashed lines in the plots. The falloff condition for the reference state at $V_f = 0.20$ may be used to evaluate the parameters λ and q (foreshadowed in Eq. (18), Part I), as follows. Inserting $\Lambda = 180$ μm at $l = 4.0$ μm (Eq. (17c), Part I) into Eq. (3b), we obtain $\varepsilon_\xi = 0.067$. Inserting ε_ξ into Eq. (5), along with $\eta = 4$ and $\mu = 2.7$ (Sect. III(2), Part I), plus $\sigma_R = 7.7$ GPa (Eq. (19a), Part I) and $E' = 300$ GPa[12] for our reference material, yields $\varepsilon_\delta = 0.013$. Then from Eq. (3$a$) (again neglecting any variation in E' with V_f) we have $\lambda/l^2 = 0.44$ μm^{-1}, which enables us to determine λ, and thence q (Eq. 17b), Part I), for each prescribed l.

With this parameter calibration, it is one further step to evaluate the limiting particle sizes l^{**} for spontaneous microcracking limits from Eq. (7). These limits are included as the *right*-hand vertical dashed lines for each V_f in Fig. 2.

IV. Implications Concerning Microstructural Design of Two-Phase Ceramics

(1) Effect of Microstructural Variables on Toughness Curves

It is apparent from the results in Sect. III of Part I and Sect. III above that incorporation of a second phase is an effective route to the control of toughness-curve behavior in ceramic composites. Using a reference composition to calibrate key crack bridging parameters in the T-curve relations, one may predict the effects of microstructural changes on the strength properties of a given material system. Here, we illustrate specifically with computed T-curves for a range of hypothetical volume fractions V_f and particle sizes l for our Al_2O_3/Al_2TiO_5 system. However, the generality of the theoretical analysis extends to potential variations in the internal mismatch stress σ_R (as modified, for instance, by incorporating a different second phase, or even changing the matrix).

(A) Volume Fraction (or Residual Stress): Consider first the influence of volume fraction V_f (or σ_R) on the T-curve. In Fig. 4 we generate $T(c)$ curves (Eqs. (6) and (8), Part I) by evaluating p and q for $V_f = 0.10$, 0.20, 0.30, and 0.40 in accordance with Eq. (1) above, keeping λ and Λ in Eq. (3) constant at the values determined for $l = 4.0$ μm (Eqs. (17c) and (18a), Part I). We see that the slope and upper plateau of the curves are enhanced, and the minimum simultaneously depressed, with increasing V_f. At the same time, the range of crack sizes over which $T(c)$ varies remains essentially constant. A conspicuous manifestation of this fixed range is the crossover of all curves through a common intersection point at $c = c_+ = 1100$ μm, $T = T_0 = 2.75$ MPa·m$^{1/2}$. Note that on substituting $T = T_0$ into Eq. (9) of Part I we obtain $c_+ = 2(1 + q/p)^2\lambda = 2(1 + 1/\eta\mu\varepsilon_\xi)^2\lambda$, which is indeed independent of V_f.

Now suppose a proportion of the natural flaw population to have initial sizes $c = c_f$ to the right of the minimum of any given curve in Fig. 4. The stability of such flaws under an applied stress σ_A is then determined by the disposition of $K_A(c) = \psi\sigma_A c^{1/2}$ relative to the shaded line passing through both the common intersection point ($c = c_+$, $T = T_0$) and the origin (cf. Fig. 1). This "transition" line corresponds to a critical volume fraction $V_f = V_f^* = 0.21$ ($l = 4.0$ μm) in the zero-intercept linear T–$c^{1/2}$ function in Eq. (9) of Part I. In keeping with the description in Sect. II(2), we distinguish two regions of material response:

(i) At $0 < V_f < V_f^*$, the equilibrium configuration $K_A = \psi\sigma_A c_f^{1/2} = T$ is unstable; failure occurs from a single, critical flaw. Note, however, that as V_f approaches V_f^* the strength becomes increasingly insensitive to c_f.

(ii) At $V_f^* < V_f$, the equilibrium at $K_A = T$, $c = c_f$ is stable, and extension proceeds up the T-curve with increasing stress until the tangency condition $dK_A/d(c^{1/2}) = dT/d(c^{1/2})$ is met. As V_f increases further beyond V_f^* the potential increases for multiple flaw extension and coalescence, with consequent strength degradation.[9]

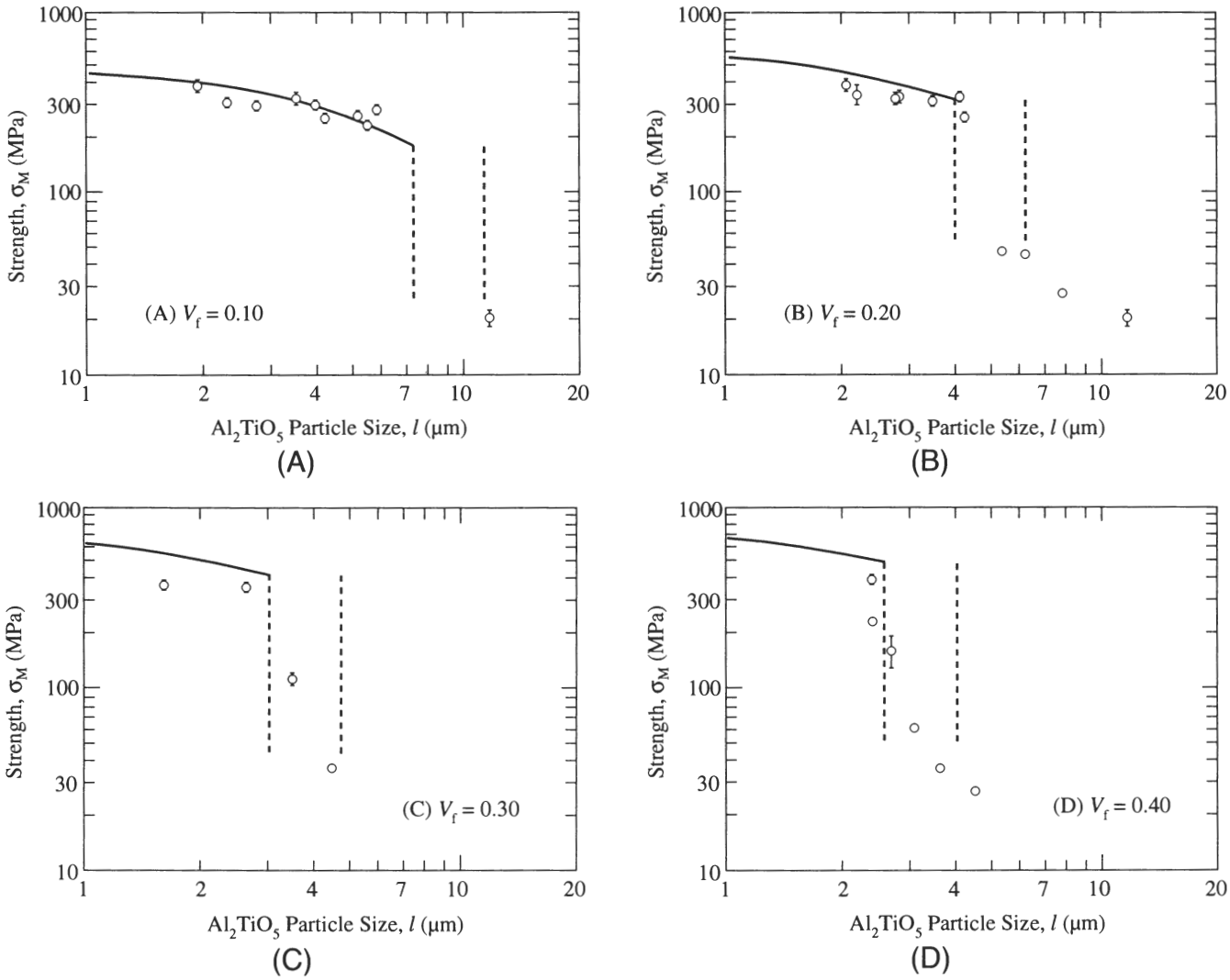

Fig. 2. Strength as function of particle size l for Al_2O_3/Al_2TiO_5 composite, for volume fractions (A) $V_f = 0.10$, (B) $V_f = 0.20$, (C) $V_f = 0.30$, (D) $V_f = 0.40$, at fixed indentation load $P = 5$ N. Error bars on datum points are standard deviations; datum points without error bars are individual results. Solid curves are generated from theoretical analysis in Part I. Vertical dashed curves indicate limiting particle sizes l^* and l^{**} evaluated from Eqs. (5) and (7).

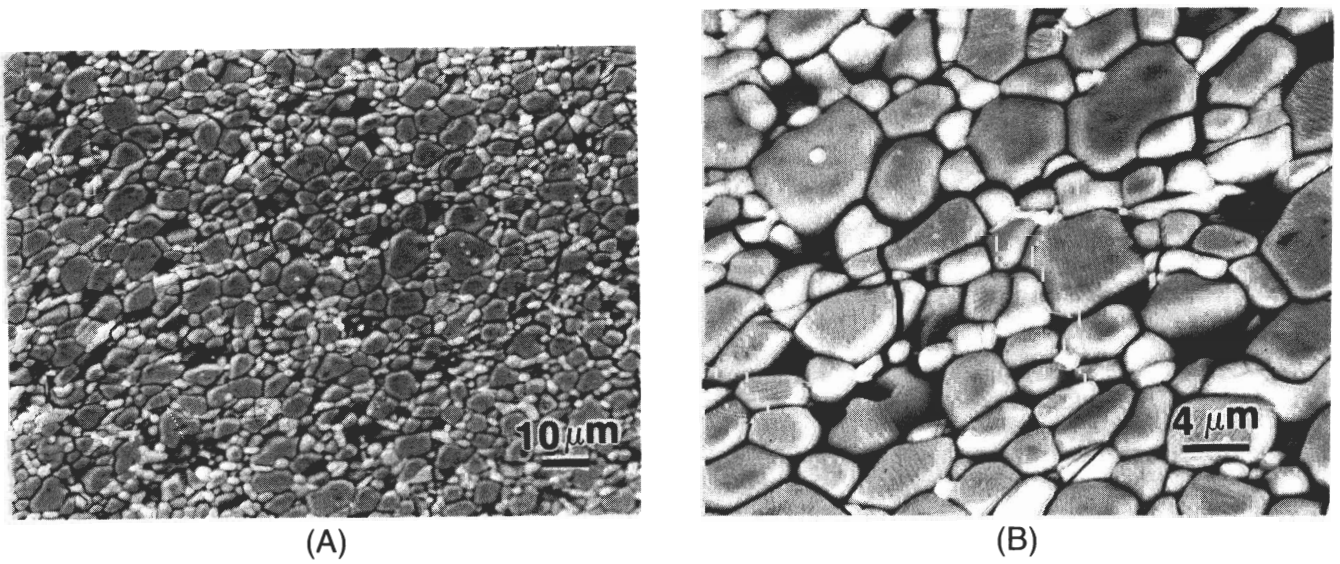

Fig. 3. SEM micrograph showing bulk microcracking damage in Al_2O_3/Al_2TiO_5 composite, $V_f = 0.30$, $l = 5.0$ μm (cf. Fig. 2(C)). Micrograph (B) is enlargement of portion of (A).

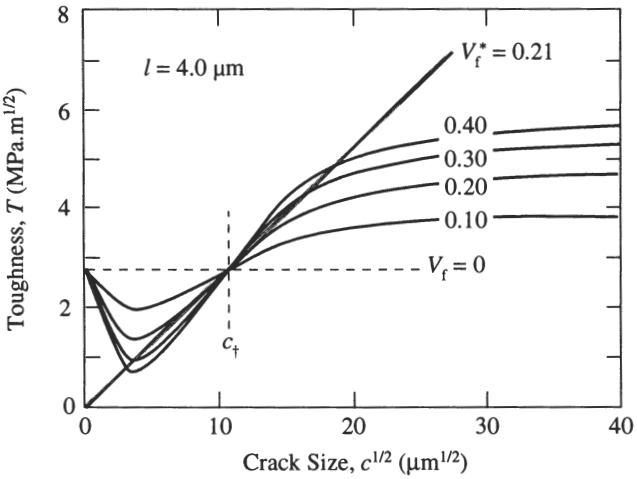

Fig. 4. Predicted T-curves for Al_2O_3/Al_2TiO_5 composites, for specified volume fractions V_f at fixed particle size $l = 4.0$ μm. Shaded line is K_A-field at $c = c_+, T = T_0$.

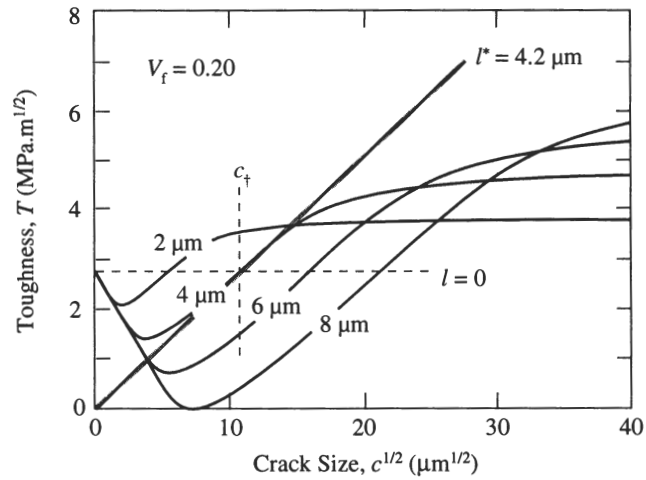

Fig. 6. Predicted T-curves for Al_2O_3/Al_2TiO_5 composites, for specified particle sizes l at fixed volume fraction $V_f = 0.20$. Shaded line is K_A-field at $c = c_+, T = T_0$.

Note that none of the curves for the $l = 4.0$ μm material in Fig. 4 intersect the c-axis, nor is there much scope for further increase in volume fraction. Thus, whereas *activated* microcracking occurs at $V_f > 0.21$, *spontaneous* microcracking strictly should not occur in the material at this particle size. However, as indicated in Sect. III(2) above, some premature flaw pop-in may be induced at the higher volume fractions by prolonged exposure to moisture.

The flaw tolerance characteristics implied in Fig. 4 are more clearly demonstrated by calculating strength as a function of initial flaw size, $\sigma_F(c_f)$, using the conventional strength formalism for natural flaws (i.e., Eqs. (13) and (14), Part I, at $\chi = 0$) within the domain $0 < V_f < V_f^*$. Figure 5 shows the results of such calculations for specified values of V_f ($l = 4.0$ μm). Consistent with the T-curve description, enlarging V_f enhances the "plateau", without affecting the extreme long-crack or short-crack strengths.

(B) Particle Size: Now consider the effect of particle size l on $T(c)$. In Fig. 6 we generate $T(c)$ functions by adjusting λ and Λ for $l = 2$, 4, 6, and 8 μm using Eq. (3) above, keeping p and q constant at the values determined for $V_f = 0.20$ (Eqs. (17a) and (18b), Part I). Observe that the slope of the "linear" region of the T–$c^{1/2}$ plot is now invariant, reflecting the independence of p and q in Eq. (9) of Part I on l. On the other hand, the upper plateau toughness *is* enhanced by increasing the particle size. Most significantly, the linear region of the curve translates to the right of the diagram and extends over a greater range of crack sizes, as l (thus λ and Λ) increases.

Suppose again that a proportion of the population of natural flaws had initial size $c = c_f$ to the right of the minimum of the pertinent curve in Fig. 6. The flaw stability is determined by the disposition of $K_A(c)$ relative to the shaded line at a critical particle size $l = l^* = 4.2$ μm ($V_f = 0.20$). Again, we distinguish two regions of material response relative to this transition line:

(i) At $0 < l < l^*$, the equilibrium is unstable, and failure occurs from a single flaw. The strength becomes increasingly insensitive to initial flaw size c_f as l approaches l^*.

(ii) At $l^* < l$, the equilibrium is stable, and the flaws extend at increasing stress up the T-curve to failure at the tangency point. Several flaw sources may be activated. As l increases further, toward and beyond l^{**}, the flaws ultimately coalesce, and strength is degraded.

Figure 7 shows calculated strength as a function of natural flaw size, $\sigma_F(c_f)$, for specified values of l within $0 < l < l^*$ ($V_f = 0.20$). Enlarging l depresses the strength plateau, but this is compensated by expansion of the "plateau" range, with attendant enhancement of the long-crack strength. A similar tradeoff

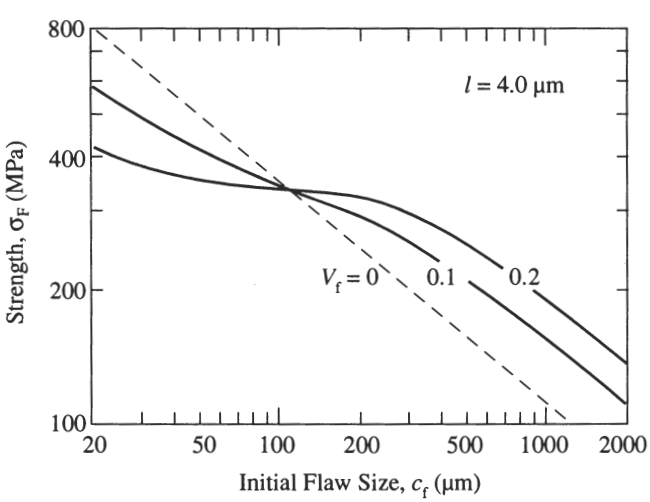

Fig. 5. Predicted strength as function of initial size of natural flaws for Al_2O_3/Al_2TiO_5 composites, for specified volume fractions V_f at fixed particle size $l = 4.0$ μm.

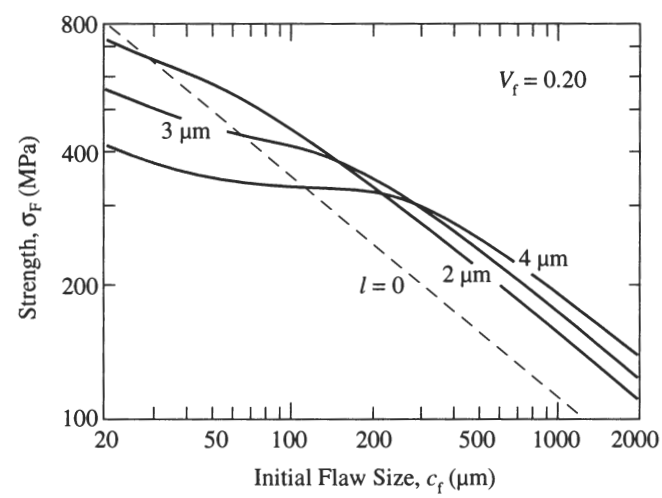

Fig. 7. Predicted strength as function of initial size of natural flaws for Al_2O_3/Al_2TiO_5 composites, for specified particle sizes l at fixed volume fraction $V_f = 0.20$.

is evident in an earlier study of the effect of grain size on strength in base alumina.[10]

(2) *Microcracking Limits and Design Criteria*

In noting how key microstructural parameters enhance certain characteristics of the *T*-curve, let us recall an interesting dichotomy foreshadowed in Sect. II(1): an increased volume fraction V_f (or residual stress σ_R) enhances the *slope*, but not the scale (Fig. 4); an increased particle size l enhances the *scale*, but not the slope (Fig. 6). We also recall that excessive increases can lead to bulk microcracking and ultimate strength degradation. It follows that control of these vital microstructural parameters should be an important element in materials design.

In this context, it is useful to consider the *design diagram* in Fig. 8, plotted as $V_f(1 - V_f)\sigma_R$ (governed by stresses p and q) vs l (governed by dimensions λ and Λ). Accordingly, the ordinate measures the *slope* of the *T*-curve, the abscissa the *scale*. The curves represent the simple inverse relations Eqs. (5) (inner curve) and 7 (outer curve). This diagram may be usefully considered in relation to the three domains of material behavior identified in Sect. II(2).

(A) No Microcracking (NM): Within the subcritical domain $V_f < V_f^*$, $l < l^*$ in Figs. 4 and 6, failure is unstable from a single flaw at $c = c_f$. However, the traditional "Griffith" condition $\sigma_F \propto c_f^{-1/2}$ is valid only for materials with single-valued toughness, corresponding to the fine-grain matrix material at $V_f = 0$ in Fig. 5 and $l = 0$ in Fig. 7. A true Griffith response is therefore realized only at the origin of Fig. 8. As V_f and l grow larger, the material becomes more flaw-tolerant, in the manner of Figs. 5 and 7, and the composite material migrates away from the origin along an appropriate configurational path in Fig. 8.

(B) Activated Microcracking (AM): For systems just at the critical condition $V_f = V_f^*$, $l = l^*$ on the inner curve in Fig. 8, the equilibrium is neutral and the critical flaw undergoes precursor extension along the linear portion of the T–$c^{1/2}$ curve, to ultimate failure at $c = \Lambda + \lambda$ (cf. Fig. 1). Now σ_F is altogether independent of c_f. As one progresses further beyond the inner curve and toward the second curve the equilibrium becomes stable, promoting the incidence of multiple flaw extensions. Strength σ_F remains independent of c_f but is compromised by any coalescence. This is the domain of stress-induced damage accumulation.

(C) Spontaneous Microcracking (SM): At $V_f > V_f^{**}$, $l > l^{**}$, small flaw sources may pop-in spontaneously from the left unstable branch to the right stable branch of the *T*-curve (e.g., at $l = 8$ μm for the $V_f = 0.2$ material in Fig. 6). Damage is therefore accumulated even in the absence of an external stress.

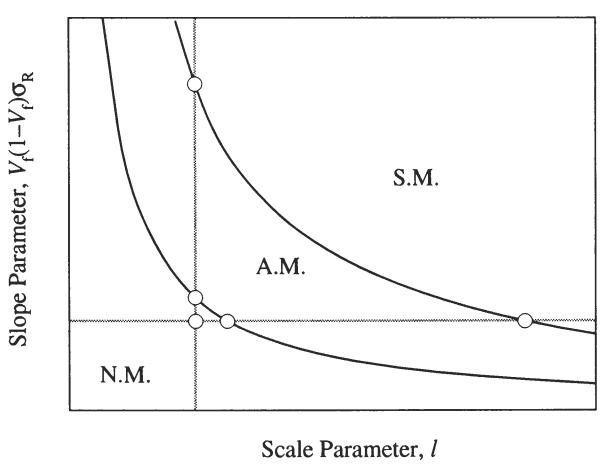

Fig. 8. "Design diagram." Curves are loci of Eqs. (5) and (7), delineating regions of *no* microcracking (N.M.), *activated* microcracking (A.M.), and *spontaneous* microcracking (S.M.). Horizontal shaded line is constant volume fraction and residual stress line; vertical shaded line is constant particle size line.

Again, in the presence of moisture, this state may develop prematurely (Sect. III(2)).

To illustrate the design utility of Fig. 8, let us consider variations in microstructural states along the two shaded lines. These two shaded lines correspond to the two principal microstructural modifications considered in this study: along the *vertical* line, to volume fraction V_f (or residual stress σ_R), as envisaged in Fig. 4; along the *horizontal* line, to particle size l, as envisaged in Fig. 6. In both cases, translation along the line away from the axes corresponds to increased flaw tolerance, limited first by activated then spontaneous microcracking damage as one intersects the two curves. There is a tradeoff here: increasing V_f (or σ_R) progressively restricts the range of l over which flaw tolerance may be achieved, and vice versa.

This latter tradeoff is implicit in the strength vs flaw-size plots for our Al_2O_3/Al_2TiO_5 composites in Figs. 5 and 7. There, we have achieved a degree of flaw tolerance by increasing V_f and l, but the relatively high value of σ_R for this material restricts the range of flaw sizes axis over which the "plateau" strength can be sustained without microcracking.

V. Discussion

The simplistic model presented in Parts I and II of this study provides us with a physical basis for predicting the influence of important microstructural variables, notably volume fraction V_f, particle size l, and thermal expansion mismatch stress σ_R, on toughness-curve and strength properties of two-phase ceramics that exhibit grain-sliding bridging. Especially insightful is the distinction made between the influences of V_f (and σ_R) on the *slope* characteristics (Fig. 4) and l on the *scale* characteristics (Figs. 6 and 7) of the *T*-curve. This dichotomy may be usefully applied in the microstructural tailoring of optimal flaw-tolerant ceramics for specific structural applications, accordingly to whether the principal requirement is for preservation of plateau strength *level* (increased V_f, Fig. 5) or enhancement of plateau *range* (increased l, Fig. 7).

The analysis also imposes limits on the potential benefits of compositional tailoring by the onset of bulk microcracking. These limits arise naturally in the model from the central role of internal residual mismatch stresses in the bridging micromechanics. They are most usefully demonstrated in the design diagram construction of Fig. 8. In that diagram, the neutral equilibrium state defined by the inner curve represents a locus of optimum flaw tolerance. Beyond that limit, flaw tolerance is retained and damage can accumulate; but strength may be lost, from activation and ultimate coalescence of multiple microcrack sources. Beyond the outer curve in Fig. 8, bulk microcracking occurs spontaneously, and loss of structural integrity may be severe. This takes us into the province of refractories, where the characteristics of individual microcracks (as introduced for example in thermal shock) become subsidiary to those of the integrated, interactive population. There, the stochastics of microcrack sources and mechanisms of coalescence are governing factors.[13,14] In these microcracking domains, the tendency to enhanced local microcracking can be highly deleterious to microfracture-induced wear resistance.[15]

The quantitative capacity of our fracture mechanics model as a predictive tool is limited by approximations in the starting equations. We have mentioned that the elliptical-crack profile relations in Eq. (3) are not self-consistent with the *K*-field solutions of Sect. III(1) in Part I. A self-consistent solution to the nonlinear displacement-field integral equations[2] could indeed be obtained by direct integration over the constant bridging stress domains of Fig. 3 in Part I, but at the sacrifice of physical insight. Such a solution will inevitably lead to relations for λ and Λ that depend on V_f as well as on l. Under such conditions *slope* and *scale* characteristics of the *T*-curve may no longer be varied independently via respective adjustments to volume fraction and particle size (as implied, for instance, in Figs. 4 and 6).

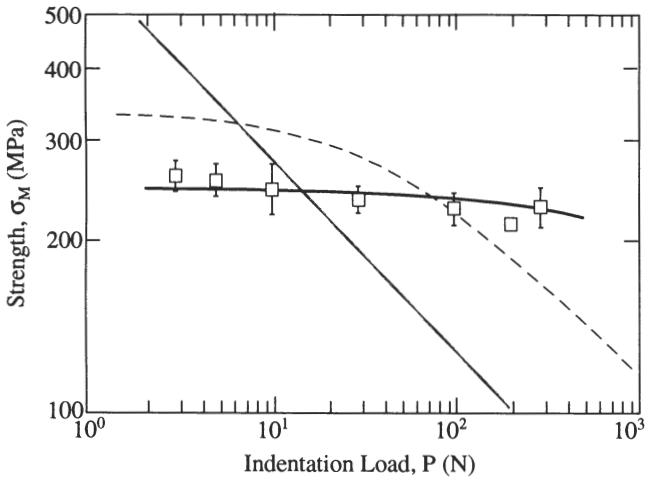

Fig. 9. Indentation–strength data for Al_2O_3/Al_2TiO_5 composite, for volume fraction $V_f = 0.20$ but with exaggerated matrix Al_2O_3 grain size and agglomerated distributions of Al_2TiO_5 particles. Data from Refs. 6 and 16. Solid curve is empirical fit to data. Compare shaded curve for base fine-grain alumina, and dashed curve for homogeneous material at same V_f (from Fig. 6, Part I).

Furthermore, the approximation of constant stress domains in the constitutive stress–separation function $s(u)$ (Fig. 2, Part I) is clearly oversimplistic; in real ceramics, $s(u)$ is tail-dominated.[16] The attendant discontinuities in $s(r)$ at $r = c - \lambda$ and $c - (\Lambda + \lambda)$ (Fig. 3, Part I) could even lead to unphysical, non-unique crack profile solutions.[4,5,17] More detailed analyses will inevitably cause changes in the shapes of the T-curves (Figs. 4 and 6) and the strength plateaus (Figs. 5 and 7). In general, therefore, we must expect the crucial rising portion of the toughness function to be considerably more complex than the "linear" T–$c^{1/2}$ representation of Eq. (9) in Part I. In this context our calibrations of the principal microstructural parameters, stresses p and q and dimensions Λ and λ, are subject to considerable uncertainty. One must exercise due care when using such calibrations as a basis for mechanical design, especially when extrapolating into the short-crack and long-crack regions beyond the data range. On the other hand, these parameters remain useful guides to the strength of the underlying bridging processes responsible for the toughening behavior.

The present study is also subjected to material-specific restrictions, from the imposition of bulk microcracking limits at relatively small particle sizes. These restrictions are attributable to the large residual mismatch stresses in our Al_2O_3/Al_2TiO_5 composites. Consequently, the current examination of flaw tolerance effects have been confined to a small range of particle sizes (Fig. 2). A more comprehensive study calls for material system with greater flexibility in the capacity to vary the microstructural variables. Such a system might include contributions to the T-curve from the matrix itself. In the present case of an alumina matrix, the contributions may become significant for grain sizes above ≈ 10 μm.[10] It has in fact been demonstrated elsewhere that deliberate incorporation of coarse matrix grains into Al_2O_3/Al_2TiO_5 composites can produce further (multiplicative) enhancements of the T-curve.[18] Inhomogeneous distributions of the second phase, e.g., by agglomeration of the aluminum titanate particles, can also enhance the toughness and flaw-tolerance properties. This latter is seen in Fig. 9.[9,19] Such spatial variability in microstructural characteristics might prove to be of even greater importance than variability in flaw size in accounting for observed scatter in strength data in flaw-tolerant ceramics, and thus become a critical issue in the processing of ceramic components for increased reliability.[9]

Acknowledgments: The authors acknowledge stimulating discussions with H. Cai and E. R. Fuller, Jr.

References

[1]B. R. Lawn, N. P. Padture, L. M. Braun, and S. J. Bennison, "Model for Toughness Curves in Two-Phase Ceramics: I, Basic Fracture Mechanics," *J. Am. Ceram. Soc.*, **76** [9] 000–000 (1993).

[2]I. N. Sneddon and M. Lowengrubb, *Crack Problems in the Classical Theory of Elasticity*. Wiley, New York, 1969.

[3]B. Budiansky, J. C. Amazigo, and A. G. Evans, "Small-Scale Crack Bridging and the Fracture Toughness of Particulate-Reinforced Ceramics," *J. Mech. Phys. Solids*, **36** [2] 167–87 (1988).

[4]B. N. Cox and D. B. Marshall, "The Determination of Crack Bridging Forces," *Int. J. Fract.*, **49**, 159–76 (1991).

[5]K.-T. Wan and B. R. Lawn, "Effect of Chemical Interaction on Barenblatt Crack Profiles in Brittle Solids," *Acta Metall.*, **40** [12] 3331–37 (1992).

[6]B. R. Lawn, *Fracture of Brittle Solids*. Cambridge University Press, Cambridge, U.K., 1993.

[7]E. Smith, "The Size of the Fully Developed Softening Zone Associated with a Crack in a Strain-Softening Material. I. A Semi-Infinite Crack in a Remotely Loaded Infinite Solid. II. A Crack in a Double-Cantilever Beam Specimen," *Int. J. Eng. Sci.*, **27** [3] 301–307, 309–14 (1989).

[8]F. Erdogan and P. F. Joseph, "Toughening of Ceramics through Crack Bridging by Ductile Particles," *J. Am. Ceram. Soc.*, **72** [2] 262–70 (1989).

[9]J. L. Runyan and S. J. Bennison, "Fabrication of Flaw-Tolerant Aluminum-Titanate-Reinforced Alumina," *J. Eur. Ceram. Soc.*, **7**, 93–99 (1991).

[10]P. Chantikul, S. J. Bennison, and B. R. Lawn, "Role of Grain Size in the Strength and *R*-Curve Properties of Alumina," *J. Am. Ceram. Soc.*, **73** [8] 2419–27 (1990).

[11]L. M. Braun, S. J. Bennison, and B. R. Lawn,"Objective Evaluation of Short-Crack Toughness Curves Using Indentation Flaws: Case Study on Alumina-Based Ceramics," *J. Am. Ceram. Soc.*, **75** [11] 3049–57 (1992).

[12]N. P. Padture, "Crack Resistance and Strength Properties of Some Alumina-Based Ceramics"; Ph.D. Dissertation. Lehigh University, Bethlehem, PA, 1991.

[13]G. Sines and T. Okada, "Flaws Responsible for Slow Cracking in the Delayed Fracture of Alumina," *J. Am. Ceram. Soc.*, **66** [3] 228–32 (1983).

[14]T. Okada and G. Sines, "Crack Coalescence and Microscopic Crack Growth in the Delayed Fracture of Alumina," *J. Am. Ceram. Soc.*, **66** [10] 719–25 (1983).

[15]S.-J. Cho, B. J. Hockey, B. R. Lawn, and S. J. Bennison, "Grain-Size and *R*-Curve Effects in the Abrasive Wear of Alumina," *J. Am. Ceram. Soc.*, **72** [7] 1249–52 (1989).

[16]Y.-W. Mai and B. R. Lawn, "Crack-Interface Grain Bridging as a Fracture Resistance Mechanism in Ceramics: II, Theoretical Fracture Mechanics Model," *J. Am. Ceram. Soc.*, **70** [4] 289–94 (1987).

[17]B. N. Cox and D. B. Marshall, "Stable and Unstable Solutions for Bridged Cracks in Various Specimens," *Acta Metall.*, **39** [4] 579–89 (1991).

[18]N. P. Padture, S. J. Bennison, and H. M. Chan, "Flaw-Tolerance and Crack-Resistance Properties of Alumina–Aluminum Titanate Composites with Tailored Microstructures," *J. Am. Ceram. Soc.*, **76** [9] 2312–20 (1993).

[19]S. J. Bennison, N. P. Padture, J. L. Runyan, and B. R. Lawn, "Flaw-Insensitive Ceramics," *Philos. Mag. Lett.*, **64** [4] 191–95 (1991). □